Short Communication

Effect of TiCl$_4$ Treatment on Different TiO$_2$ Blocking Layer Deposition Methods

Vladyslav Ostapchenko, Qiyu Huang[*]*, Qing Zhang, and Chuanrui Zhao*

Department of Micro/Nano-Electronics, Shanghai Jiao Tong University, Shanghai 200240, China
[*]E-mail: qiyu@sjtu.edu.cn

Organolead halid perovskite CH$_3$NH$_3$PbI$_3$ solar cells with all-mesoporous device structure were fabricated with TiO$_2$ blocking layer created by two different methods. Three groups of devices were tested. The TiO$_2$ blocking layer of group 1 was spin-coated with conventional method, while that of groups 2 and 3 was grown by magnetron sputtering of metallic Ti and followed thermal oxidation. Different durations (0, 30, 45, and 60 minutes) of TiCl$_4$ treatment were used during fabrication to study how the performance of each group of solar cells was affected. For all groups of samples, it was obvious that treated samples had much better I-V characteristics that non-treated, with up to 50% improvement in PCE. The difference in the performance improvement was investigated.

1. INTRODUCTION

Over the past few years, perovskite solar cells (PSCs) showed rapid increase in power conversion efficiencies (PCEs) from the initial 3.8% in 2009 [1] up to the certified 20.1% in 2016 [2]. Such high results were achieved by using *methylammonium* lead halide perovskite as light absorber, which is a material with high light harvesting, decent optical and electric properties [3]. PSC device structure was originally similar to that of a dye-sensitized solar cell (DSSC). But later better results were obtained with a solid state device structure, in which Spiro-MeOTAD acted as hole transport material (HTM) and thermally evaporated gold or platinum as counter electrode [4]. Since then, there have been many attempts of optimization on the device structure and layer materials of PSC to simplify the fabrication process along with improving PCE and make this type of solar cells competitive in future commercialization. Good results were obtained by using low cost conductive materials such as graphite, carbon black (CB) or their mixture as counter electrode (CE) [5]. Even by

using mesoporous HTM-free structure PSC, several researchers [6] managed to reach 12% PCE. Good results were also achieved by employing mesoporous Nickel Oxide (NiO) particles in an attempt to replace high-cost organic HTM, Spiro-MeOTAD. NiO has been one of successful candidates for p-type contact since DSSCs [7] and has good ambipolar charge transport behavior, which makes it suitable for HTM layer in PSCs as well [8].

In this work, we used an all-mesoporous-layer structure for PSCs, employing inexpensive mesoporous materials: TiO_2 layer acting as electron transport layer (ETL), Al_2O_3 as spacer layer, NiO as HTM and carbon black-graphite mixture as CE. Mesoporous inorganic metal oxide layers along with carbon black-graphite CE acted as scaffold, which was infiltrated with perovskite (MAPbI3). TiO_2 acted as electron selective contact, while NiO acted as hole extraction layer. Spacer layer was applied to reduce the hole-electron recombination and acted as an extra layer to prevent shortcuts between CE and FTO as well. There were a few reports showing good results with this structure, achieving up to 15% PCE [9-11].

Special attention needs to be paid on the preparation of TiO_2 compact layer, which is sometimes called blocking or dense layer. It is crucial for high PCEs by preventing recombination processes [12]. Along with commonly used technique of spin coating TiO_2 colloid precursor [13], TiO_2 blocking layer formed by thermal oxidation of sputtered metallic Ti layer was also compared. It was believed to be a cheap and fast technique of applying blocking layer since first reported [14]. TiO_2 blocking layer is an important part of ETL and along with mesoporous TiO_2 layer is crucial in achieving high efficiencies [15].

It is a common practice to apply a special $TiCl_4$ treatment to TiO_2 layer to increase the ETL quality and reduce charge recombination [16-18]. There were several reports of studying $TiCl_4$ treatment effect on TiO_2 layer for traditional PSC structure [19, 20]. However, not much information about how this treatment influenced all-mesoporous structure PSCs was reported. In this work, we compared the influence of treatment time on PCE of all-mesoporous structure PSCs, using TiO_2 blocking layer deposited by different deposition techniques.

2. EXPERIMENTAL

2.1. All-mesoporous layer pastes

Mesoporous TiO_2 paste: The mixture consisted of 2.84 g ~21 nm nanoparticles of TiO_2 (P25, HeptaChroma), 1.42 g of ethyl cellulose, 11.5 g terpineol, and 60 ml of ethanol. It was put into a 100 ml cup of a ball-milling machine and milled at 150 rpm for 24 hours.

Al_2O_3 paste: The mixture consisted of 3 g ~20 nm nanoparticles of Al_2O_3, 1.5 g of ethyl cellulose, 10 g terpineol, and 30 ml of ethanol. It was put into a 100 ml cup of a ball-milling machine and milled for 2 hours at 250 rpm. After ball-milling, the resulting paste tended to be gel-like, which was hard for spin-coating. Therefore, another 20 ml of ethanol was added to cup and ball-milled for 3 min.

NiO paste: The mixture consisted of 3 g ~20 nm NiO nanoparticles, 1.5 g of ethyl cellulose, 10

g terpineol, and 20 ml of ethanol. It was put into a 100 ml cup of a ball-milling machine and milled at 250 rpm for 2 hours.

CE paste: The mixture consisted of 6 g 8000 mesh graphite particles, 0.6 g of multi-walled carbon nanotubes (MWCNT) (with avg. size of 10 nm and the length of 8 μm), 0.3 g of CB, 0.6 g of ethyl cellulose and 42 g terpineol. It was put into a 100 ml cup of a ball-milling machine and milled at 250 rpm for 2 hours.

2.2. ETL layer fabrication

Fluorine doped indium tin oxide (FTO) glass with FTO layer thickness of 400 nm (Zhuhai Kaivo) was cleaned with ethanol and sonicated in DI water for 20 min. After drying in air, it was UV-treated for another 20 min. For the samples in group 1, 0.25 M solution of 97% Titanium(IV) isopropoxide (TiIP) (Aldrich) in n-Butanol was spin-coated twice at a speed of 3000 rpm for 15 sec, with drying on a 150 °C hot plate in between. The FTO samples in groups 2 and 3 were magnetron-sputtered with 10 nm and 30 nm of Ti respectively. All three groups of samples were spin-coated twice at 5000 rpm for 15 sec with mesoporous TiO_2 paste at room temperature, with drying on a 150°C hot plate in between. After that, they were annealed in a 550 °C oven for 30 min. With this one-step sintering process, both blocking and mesoporous were annealed together, which was beneficial to the improvement of the interfacial contact. Samples were cooled down slowly at about 1 °C/min to avoid crack generation. Sputtered samples became transparent after annealing, which indicated the successful oxidation of metal Ti to TiO_2.

2.3. TiCl$_4$ treatment

0.04 M of 99% $TiCl_4$ solution was prepared by first slowly dropping $TiCl_4$ over 50 g DI water (Deionized water) ice and then diluted with 250 ml DI water in a 300 ml vessel at room temperature. The samples, already covered with dense and mesoporous TiO_2, were placed into the $TiCl_4$ solution in the 300 ml vessel on hot plate, keeping the temperature of solution to be 70 °C. The temperature of the solution was monitored by a dip-in thermometer. All samples were placed in same vessel, facing up. Time countdown started as soon as the solution reached 70 °C. When the finishing time reached for a specific group of samples, they were taken out, rinsed with DI water, and blow-dried in N_2 flow at room temperature. After all samples were dried, they were annealed again in the 550 °C oven for 30 min.

2.4. Device fabrication

Before each coating, samples were dehydrated at 150 °C hot plate and then cooled down to room temperature. $TiCl_4$ treated samples were first covered with Al_2O_3 spacer layer by spin coating at 3000 rpm for 15 sec. After that, NiO was spin-coated twice at 5000 rpm for 15 sec. Finally, graphite-

CB counter electrode contact was spin-coated twice, each at 3000 rpm for 15 sec. After the final drying on 150°C hot plate, the samples were annealed at 400 °C for 30min to remove all organic components in pastes and create mesoporous structure.

After slow cool-down, the 2-step process of perovskite deposition was employed as stated in [21]. Briefly, first the all-mesoporous samples were infiltrated with 1 M solution of PbI_2 in DMF (Dimethylformamide), by spin-coating at 6000 rpm for 17 sec. After being dried on 110°C hot plate for 20 min, the samples were cooled down to room temperature and placed in 7 mg/ml Methyl Amonium Iodide (MAI) solution in 2-propanol. The process of MAI synthesis can be found elsewhere [22]. After 30 min of soaking, samples with infiltrated and fully converted perovskite were rinsed with 2-propanol, dried, and ready to be tested.

2.5. Device characterization

I-V tests were carried out under one sun-calibrated solar simulator (CHF-XM-500W, Beijing Trusttech Co., Ltd.) with AM 1.5G spectra filter. CHI-660D (CH Instruments, Inc.) electrochemical workstation was used to perform photovoltaic measurement. The serial resistance (R_s) and the shunt resistance (R_{sh}) were estimated from the I-V curve. SEM (scanning electron microscopy) pictures were taken using ZEISS-Ultra scanning electron microscope.

3. RESULTS AND DISCUSSION

3.1. All-mesoporous device structure
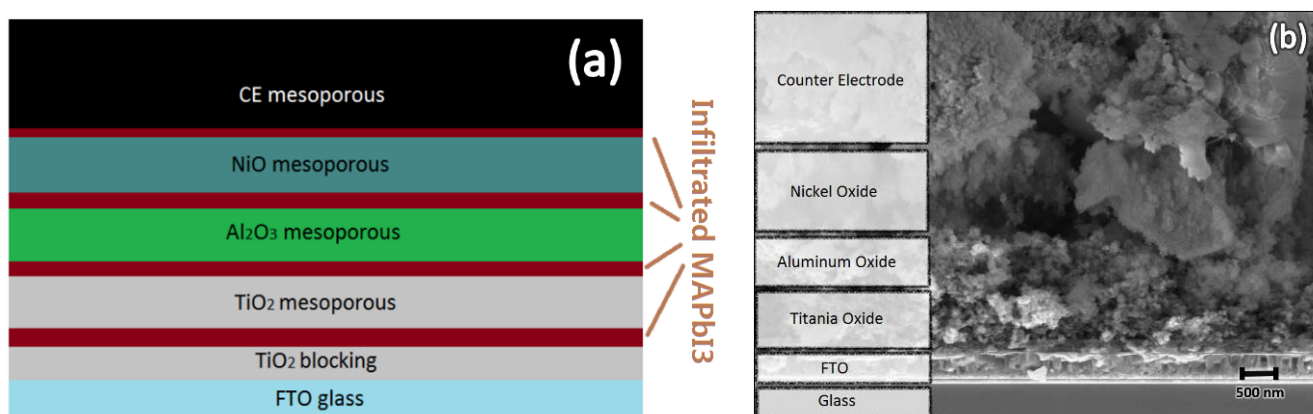
Figure 1. Illustration of the device structure: (a) schematic representation; (b) SEM image.

The device structure used in this work was illustrated in Fig. 1. Mesoporous layers of TiO_2, Al_2O_3, NiO and CE acted as scaffolds for the infiltrated perovskite material $MAPbI_3$. The total thickness was about 8 μm for all prepared samples, in which the CE was the thickest. During the optimization phase of experiment, it was found that such a thick layer of CE was necessary to achieve

high current density (J_{sc}) and high fill factor (FF). In addition, a small amount of MWCNT was added to the CE to act as bridges between graphite and carbon black particles and to improve the overall conductivity of CE. While TiO_2 acted as ETL, NiO, a type of inorganic oxide material, acted as both hole extraction layer and spacer layer at the same time [9]. NiO proved itself to be good hole selective material in DSSCs [23, 24] and was used successfully in PSC before [11, 25, 26]. Figure 2 showed a device energy level diagram. As can be seen from the figure that the NiO energy level of -5.2 eV is consistent with that of the perovskite, -5.43eV and the CE, -5 eV [11].
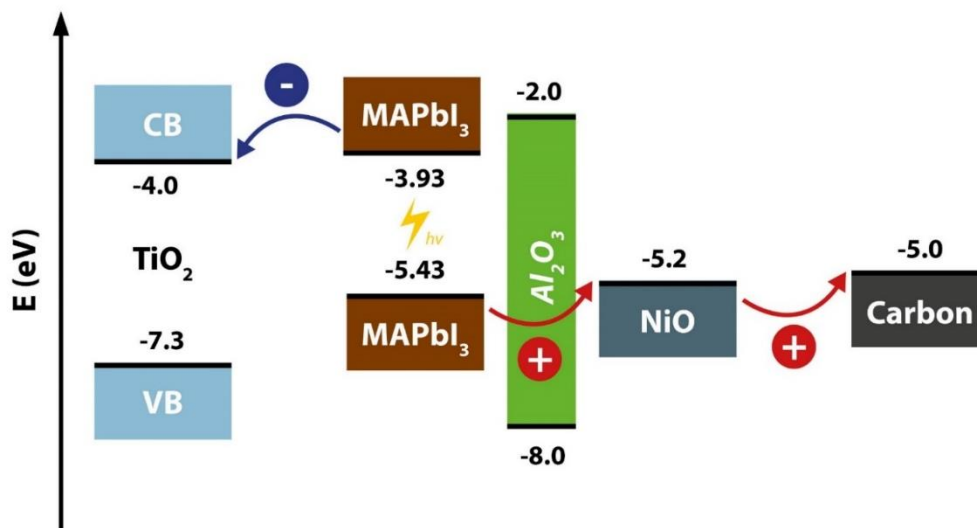

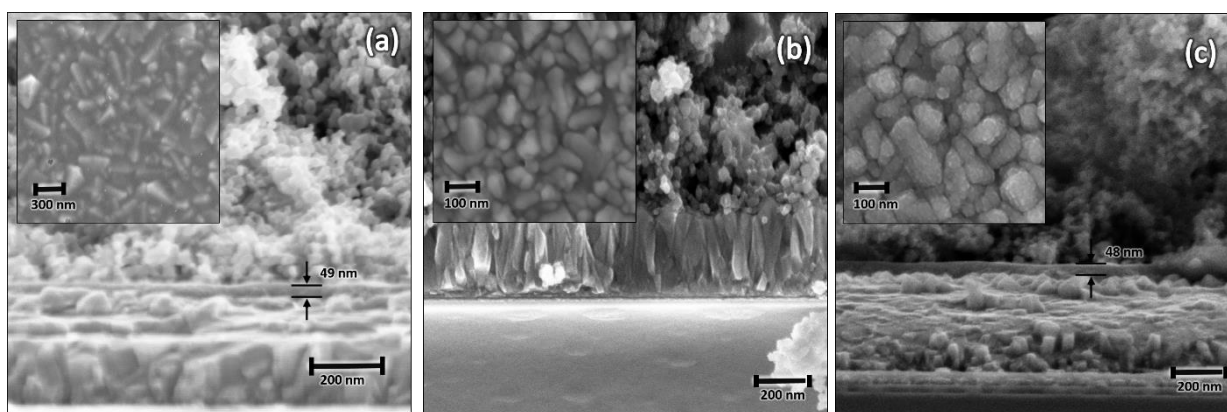**Figure 2.** Energy band diagram of the fabricated device.

Figure 3. Cross-sectional SEM images of TiO_2 blocking layers in a PSC, prepared by (a) spin-coating of TiIP; (b) 10 nm sputtered Ti; (c) 30nm sputtered Ti. The insets showed surface profiles after the TiO_2 blocking layers were deposited and annealed.

Since both NiO and CE were infiltrated with perovskite, the path for hole transport was either from perovskite through NiO to CE or to CE directly. Preliminary experiments of the layer thickness optimization revealed that thickness of NiO had significant impact to the PCE of the devices. It may be

explained by that NiO acted as a spacer layer as well, preventing the charge recombination between CE and TiO_2 [9]. For even better recombination prevention, a layer of Al_2O_3 was used. Since the energy level of Al_2O_3 is so high that it does not influence the charge separation process in the device.

Table 1. Photovoltaic characteristics of prepared samples without TiCl4 treatment.

	Voc (V)	Jsc (mA·cm^{-2})	FF	PCE (%)	Rs (ohm·cm^2)	Rsh (ohm·cm^2)
TiIP	0.934	23.198	0.38	8.242	63.241	58.8
10 nm	0.989	11.705	0.583	6.747	49.08	3351.6
30 nm	0.881	9.004	0.37	2.933	55.556	129.667

Table 2. Photovoltaic characteristics of prepared samples after $TiCl_4$ treatment

	Voc (V)			Jsc (mA·cm^{-2})			FF			PCE (%)		
	Grp 1	Grp 2	Grp 3	Grp 1	Grp 2	Grp 3	Grp 1	Grp 2	Grp 3	Grp 1	Grp 2	Grp 3
0 min	0.93	0.98	0.80	20.93	10.96	8.18	0.33	0.59	0.31	6.86	6.34	1.70
30 min	0.99	0.99	0.87	22.93	21.63	20.00	0.43	0.56	0.31	10.19	12.42	5.47
45 min	1.00	0.99	0.87	21.28	20.00	23.09	0.44	0.57	0.32	9.91	11.37	6.34
60 min	0.98	0.82	0.89	21.33	6.58	23.56	0.45	0.55	0.34	9.56	3.14	7.12

Note: Grp 1 was the samples with TiO_2 blocking layer prepared by spin-coating of TiIP; Grps 2 and 3 were the samples with TiO_2 blocking layer created by magnetron sputtering of Ti and a followed thermal oxidation.

3.2. Characterization of the blocking layer without $TiCl_4$ treatment

For an in-depth analysis of $TiCl_4$ treatment effect, three groups of samples were fabricated. Group 1 was the devices with TiO_2 blocking layer, created by spin coating of TiIP. Group 2 and group 3 were with blocking layers, created by the oxidation of 10 nm and 30 nm sputtered Ti respectively. The thickness of TiO_2 blocking layer, obtained after annealing at 550 °C in the oven was indicated in Fig. 3. SEM measurement of three groups of samples revealed that for samples in group 1 and group 3 the thickness of the blocking layer was almost same, about 48 nm. On the other hand, for the samples in group 2, the blocking layer was too thin to be easily identified between the layers of FTO crystals and mesoporous TiO_2. However, since the thickness of Ti layer in group 2 was one third of that in group 3, it would be reasonable to assume that the thickness of TiO_2 layer in group 2 was about 16 nm. All other layers were prepared in the same way for all three groups.

Photovoltaic characteristics of the devices obtained under standard AM 1.5G illumination were summarized in Table 1. It was shown that despite of the fact that samples in group 1 and group 3 had almost the same thickness of blocking layers, testing results were very different. To understand the difference among the blocking layers in these groups, it is better to compare their I-V characteristics without any $TiCl_4$ treatment, because the treatment is known to change the characteristics of TiO_2

significantly [16-18].

Even though the TiO_2 blocking layers of samples in groups 1 and 3 had almost the same thickness, the I-V characterization results differed a lot. Without any $TiCl_4$ treatment, the samples in group 1 showed significantly higher V_{oc} and J_{sc}. Since the devices in both groups had the same structure and the only difference was the blocking layer, it could only be attributed to the difference between the blocking layers in groups 1 and 3.

V_{oc} is determined by the conduction band of mesoporous TiO_2 (CB) and the electron lifetime in the CB for these two groups [27]. Since the CB positions are pretty much the same for both groups, the difference in V_{oc} can only be ascribed to the electron lifetime difference. There were two competing factors affecting the electron lifetime. On one hand, the sputtering technique created much denser and much more uniform layer, while the spin-coated samples may still have some voids or cavities [28], which meant a lot more grain boundaries for the electrons to pass through before recombination, hence an increased V_{oc}. This can also be seen from a larger R_s for group 1. On the other hand, those cavities most probably were infiltrated with perovskite material during fabrication, which meant that even though these two TiO_2 blocking layers had the same thickness, the electron collection efficiency is higher for group 1 than for group 3. This could lead to a shorter electron lifetime, hence a reduced V_{oc}, and a better charge collection, that is, a higher J_{sc}. While for samples in group 2, even though the thickness of the blocking layer was thinner than that in group 3, it was still thick enough to prevent charges from recombination, which can clearly be seen from a much larger R_{sh}. R_{sh} is closely related to the charge recombination at interfaces inside the device. The contact between the FTO and HTM is the main channel for charge recombination. In perovskite solar cells, since holes can also be stored in the perovskite layer, the contact between the FTO and perovskite should therefore also be considered, making the blocking layer more critical [29]. Similar observation was also described by Gao et. al. when comparing spin-coated and sputtered samples [28]. In another work, Ke, et. al. showed that without any $TiCl_4$ treatment, for sputtered blocking layer the optimal thickness was 15 nm, with about 15.07% PCE while for spin-coated samples the optimal thickness was 60 nm to achieve 13.47% [14].

3.3. Analysis of TiCl₄ treatment effect

The photovoltaic parameters, such as open circuit voltage (V_{oc}), short-circuit current density (J_{sc}), fill factor (FF) and power conversion efficiency (PCE), after different periods of $TiCl_4$ treatment and the impact of $TiCl_4$ treatment on the samples in groups 1, 2, and 3 were summarized in Table 2. The duration of $TiCl_4$ treatment was denoted as 0 min (no treatment), 30, 45 and 60 minutes. Usually the standard treatment duration in literature for DSSCs or PSCs was 30 min. For samples in groups 1 and 2, the best PCE result appeared at 30 min too. However, the best result for samples in group 3 in our experiment was twice longer - 60 min. One possible reason for the low PCE after 30 min for groups 1 and 2 may be the damaging of blocking layer with $TiCl_4$ solution over time, as its concentration increased over treatment time. This was in agreement with what was observed by Han, et. al. [30]. In Han's work, the XRD analysis showed that TiO_2 particles size became smaller after the treatment. However, since the samples in group 3 had a dense and thick blocking layer, the $TiCl_4$

treatment reduced the blocking layer thickness not so significantly compared to groups 1 and 2, leaving still thick enough of material to prevent charges from recombination. Therefore, I-V characteristic improved with the increased treatment time for this group.

For all groups of samples, it was obvious that treated samples had much better I-V characteristics that non-treated, with up to 50% improvement in PCE. Considering that the treatment procedure increased neither the surface area of mesoporous ETL, nor the amount of infiltrated perovskite significantly, this rise should attribute to the improved charge separation or electron collection efficiency. Electron transport in mesoporous TiO_2 was characterized by higher diffusion coefficient [31] caused by the increase in the necking of TiO_2 nanoparticles, compared to the non-treated samples [32]. The increase in the necking facilitated the percolation of electrons from one particle to another, which in turn reduced the charge recombination probability [33]. It is believed to be the main reason for the increased photocurrent density. The increasing of V_{oc} may be attributed to the reduced recombination, which leaded to the increase of electron-carrier concentration, and, in turn, to the upward shift of the electron Fermi level [34].

The difference among the three group of samples was TiO_2 blocking layer. Other than their different densities, their thickness was also different (Fig. 3(a)-(c)). Treatment of blocking layer with $TiCl_4$ was described in literature as reducing the amount of charge state traps and, hence suppressing charge recombination [35]. Also, the treatment creates more contact points between mesoporous and dense layers and improves contact interface, which in turn reduces serial resistance R_s, leading to increased J_{sc} and FF [36]. Along with photovoltaic characteristics, it was also found that $TiCl_4$ treatment of TiO_2 increased the optical path of the light, i.e. increased the refractive index of ETL [37]. However, the thicker the blocking layer is, the less transparent the film becomes, which can in turn reduce the amount of light absorbed by perovskite, as in the case for samples in group 3 with a thick and dense TiO_2 blocking layer.

4. CONCLUSION

Devices with spin-coated (group1) and sputtered and oxidized (groups 2 and 3) TiO_2 blocking layer were tested and compared versus different $TiCl_4$ treatment duration. The analysis of I-V characteristics revealed that the $TiCl_4$ treatment was beneficial for all groups of samples. Optimal time of treatment was 30 minutes for group 1 and 2. For group 3, the optimal time was 60 minutes. The reason for this difference is believed to be the damaging of TiO_2 blocking layer as treatment time increases. Since the blocking layer in group 2 was the thinnest and group 1 not dense, damage occurred earlier than for group 3 whose blocking layer was dense and thick.

Among all three groups of samples, group 2 showed the best results of 12.42% PCE. It was attributed to the fact that the samples in group 2 had the thinnest TiO_2 blocking layer, resulting in the smallest serial resistivity. Furthermore, the quality of the blocking layer in group 2 was the best. As a result, it exhibited the largest shunt resistance. As for groups 1 and 3, their TiO_2 blocking layers were almost the same thick. However, the I-V characteristics were very different due to their different densities. Group 3 had a dense and thick blocking layer, which decreased its optical transparency and resulted in the lowest PCE.

References

1. A. Kojima, K. Teshima, Y. Shirai, and T. Miyasaka, *J. Am. Chem. Soc.*, 131 (2009) 6050.
2. W. Nie, H. Tsai, R. Asadpour, J. C. Blancon, A. J. Neukirch, G. Gupta, J. J. Crochet, M. Chhowalla, S. Tretiak, and M. A. Alam, *Science*, 347 (2015) 522.
3. E. J. Juarez-Perez, R. S. Sanchez, L. Badia, G. Garciabelmonte, S. K. Yong, I. Morasero, and J. Bisquert, *J. Phys. Chem. Lett.*, 5 (2014) 2390.
4. M. Liu, M. B. Johnston, and H. J. Snaith, *Nature*, 501 (2013) 395.
5. S. N. Habisreutinger, T. Leijtens, G. E. Eperon, S. D. Stranks, R. J. Nicholas, and H. J. Snaith, *Nano Lett.*, 14 (2014) 5561.
6. J. Shi, J. Dong, S. Lv, Y. Xu, L. Zhu, J. Xiao, X. Xu, H. Wu, D. Li, and Y. Luo, *Appl. Phys. Lett.*, 104 (2014) 063901
7. E. A. Gibson, A. L. Smeigh, P. L. Le, J. Fortage, G. Boschloo, E. Blart, Y. Pellegrin, F. Odobel, A. Hagfeldt, and L. Hammarström, *Angew. Chem. Int. Edit.*, 48 (2009) 4402.
8. S. Seo, I. J. Park, M. Kim, S. Lee, C. Bae, H. S. Jung, N. G. Park, J. Y. Kim, and H. Shin, *Nanoscale*, 8 (2016) 11403.
9. K. Cao, Z. Zuo, J. Cui, Y. Shen, T. Moehl, S. M. Zakeeruddin, M. Grätzel, and M. Wang, *Nano Energy*, 17 (2015) 171.
10. M. W. Lin, K. C. Wang, J. H. Wang, M. H. Li, Y. L. Lai, T. Ohigashi, N. Kosugi, P. Chen, D. H. Wei, and T. F. Guo, *Adv. Mater. Interfaces*, (2016)
11. K. C. Wang, J. Y. Jeng, P. S. Shen, Y. C. Chang, E. W. Diau, C. H. Tsai, T. Y. Chao, H. C. Hsu, P. Y. Lin, and P. Chen, *Sci. Rep.*, 4 (2014) 560.
12. P. J. Cameron and L. M. Peter, *J. Phys. Chem. B*, 107 (2003) 14394.
13. S. M. Seetharaman, P. Nagarjuna, P. N. Kumar, S. P. Singh, M. Deepa, and M. A. Namboothiry, *Physical Chemistry Chemical Physics Pccp*, 16 (2014) 24691.
14. W. Ke, G. Fang, J. Wang, P. Qin, H. Tao, H. Lei, Q. Liu, X. Dai, and X. Zhao, *ACS Appl. Mater. Inter.*, 6 (2014) 15959.
15. J. T. Wang, J. M. Ball, E. M. Barea, A. Abate, J. A. Alexanderwebber, J. Huang, M. Saliba, I. Morasero, J. Bisquert, and H. J. Snaith, *Nano Lett.*, 14 (2014) 724.
16. A. Marchioro, A. Dualeh, A. Punzi, M. Grätzel, and J.-E. Moser, *J. Phys. Chem. C*, 116 (2012) 26721.
17. J. E. Moser, D. Noukakis, U. Bach, Y. Tachibana, D. R. Klug, J. R. Durrant, R. HumphryBaker, and M. Grätzel, *J. Phys. Chem. B*, 102 (1998) 3649.
18. S. Ardo, D. Achey, A. J. Morris, M. Abrahamsson, and G. J. Meyer, *J. Am. Chem. Soc.*, 133 (2011) 16572.
19. M. Abdi-Jalebi, M. I. Dar, A. Sadhanala, S. P. Senanayak, F. Giordano, S. M. Zakeeruddin, M. Grätzel, and R. H. Friend, *J. Phys. Chem. Lett.*, 7 (2016)
20. Z. Liu, Q. Chen, Z. Hong, H. Zhou, X. Xu, N. D. Marco, P. Sun, Z. Zhao, Y. B. Cheng, and Y. Yang, *ACS Appl. Mater. Inter.*, 8 (2016)
21. J. Burschka, N. Pellet, S. J. Moon, R. Humphrybaker, P. Gao, M. K. Nazeeruddin, and M. Grätzel, *Nature*, 499 (2013) 316.
22. D. Liu and T. L. Kelly, *Nat. Photonics*, 8 (2014) 133.

23. J. R. Manders, S. W. Tsang, M. J. Hartel, T. H. Lai, S. Chen, C. M. Amb, J. R. Reynolds, and F. So, *Adv. Funct. Mater.*, 23 (2013) 2993.
24. M. D. Irwin, D. B. Buchholz, A. W. Hains, R. Chang, and T. J. Marks, *P Natl. Acad. Sci.*, 105 (2008) 2783.
25. Z. Zhu, Y. Bai, T. Zhang, Z. Liu, X. Long, Z. Wei, Z. Wang, L. Zhang, J. Wang, and F. Yan, *Angew. Chem. Int. Edit.*, 53 (2014) 12571.
26. H. Wang, X. Y. Hu, and H. X. Chen, *RSC Adv.*, 5 (2015) 30192.
27. Z. Yu, N. Vlachopoulos, A. Hagfeldt, and L. Kloo, *RSC Adv.*, 3 (2013) 1896.
28. Q. Gao, S. Yang, L. Lei, S. Zhang, Q. Cao, J. Xie, J. Li, and Y. Liu, *Chem. Lett.*, 44 (2015) 624.
29. Y. Wu, X. Yang, H. Chen, K. Zhang, C. Qin, J. Liu, W. Peng, A. Islam, E. Bi, and F. Ye, *Appl. Phys. Express*, 7 (2014) 782.
30. Z. Han, Z. Zhao, Z. Du, L. Zhao, and X. Cong, *Mater. Lett.*, 136 (2014) 424.
31. M. J. Cass, F. L. Qiu, A. B. Walker, A. C. Fisher, and L. M. Peter, *J. Phys. Chem. B*, 107 (2003) 113.
32. S. Kambe, S. Nakade, T. Kitamura, Y. Wada, and S. Yanagida, *J. Phys. Chem. B*, 106 (2002) 2967.
33. L. Vesce, R. Riccitelli, G. Soscia, T. M. Brown, A. D. Carlo, and A. Reale, *J Non-Cryst. Solids*, 356 (2010) 1958.
34. M. Wang, J. Liu, N. L. Cevey-Ha, S. J. Moon, P. Liska, R. Humphry-Baker, J. E. Moser, C. Grätzel, P. Wang, and S. M. Zakeeruddin, *Nano Today*, 5 (2010) 169.
35. W. Xu, S. Dai, L. Hu, C. Zhang, S. Xiao, X. Luo, W. Jing, and K. Wang, *Plasma Sci. Technol.*, 9 (2007) 556.
36. S. Ito, T. N. Murakami, P. Comte, P. Liska, C. Grätzel, M. K. Nazeeruddin, and M. Grätzel, *Thin Solid Films*, 516 (2008) 4613.
37. H. Choi, C. Nahm, J. Kim, J. Moon, S. Nam, D. R. Jung, and B. Park, *Curr. Appl. Phys.*, 12 (2012) 737.